Molecular Biology of the Cell
Vol. 20, 2413–2427, May 1, 2009

Faciogenital Dysplasia Protein (FGD1) Regulates Export of Cargo Proteins from the Golgi Complex via Cdc42 Activation

Mikhail V. Egorov,* Mariagrazia Capestrano,* Olesya A. Vorontsova,† Alessio Di Pentima,* Anastasia V. Egorova,* Stefania Mariggiò,* M. Inmaculada Ayala,* Stefano Tetè,‡ Jerome L. Gorski,§ Alberto Luini,* Roberto Buccione,* and Roman S. Polishchuk*

*Department of Cell Biology and Oncology, Consorzio Mario Negri Sud, 66030 Santa Maria Imbaro (Chieti), Italy; †Laboratory of Pathomorphology, State Research Institute of Maternity and Childhood, Ivanovo 153731, Russia; ‡Department of Oral Sciences, University "G. D'Annunzio," 66013 Chieti, Italy; and §Division of Medical Genetics, Departments of Child Health and Pathology, University of Missouri School of Medicine, Columbia, MO 65212

Submitted November 20, 2008; Revised February 17, 2009; Accepted February 24, 2009
Monitoring Editor: Adam Linstedt

Mutations in the *FGD1* gene are responsible for the X-linked disorder known as faciogenital dysplasia (FGDY). *FGD1* encodes a guanine nucleotide exchange factor that specifically activates the GTPase Cdc42. In turn, Cdc42 is an important regulator of membrane trafficking, although little is known about FGD1 involvement in this process. During development, FGD1 is highly expressed during bone growth and mineralization, and therefore a lack of the functional protein leads to a severe phenotype. Whether the secretion of proteins, which is a process essential for bone formation, is altered by mutations in FGD1 is of great interest. We initially show here that FGD1 is preferentially associated with the *trans*-Golgi network (TGN), suggesting its involvement in export of proteins from the Golgi. Indeed, expression of a dominant-negative FGD1 mutant and RNA interference of FGD1 both resulted in a reduction in post-Golgi transport of various cargoes (including bone-specific proteins in osteoblasts). Live-cell imaging reveals that formation of post-Golgi transport intermediates directed to the cell surface is inhibited in FGD1-deficient cells, apparently due to an impairment of TGN membrane extension along microtubules. These effects depend on FGD1 regulation of Cdc42 activation and its association with the Golgi membranes, and they may contribute to FGDY pathogenesis.

INTRODUCTION

Membrane transport has a fundamental role in tissue biogenesis through its supply of extracellular matrix components, surface adhesion molecules, and the lipids and proteins that are essential for specific cell-surface domains (Mostov *et al.*, 2003; Nelson, 2003; Rodriguez-Boulan *et al.*, 2005). During embryonic and postnatal development, these transport events are tightly coordinated with the activities of other cellular systems (e.g., the cytoskeleton, adhesion patches) through numerous signaling proteins (Nelson, 2003; Rodriguez-Boulan *et al.*, 2005). Mutations in these regulatory proteins can therefore induce genetic disorders that are frequently accompanied by severe phenotypes.

FGD1 has been hypothesized to coordinate membrane transport and the actin cytoskeleton during embryogenesis (Estrada *et al.*, 2001), and it has been implicated in skeletal development, with mutations in *FGD1* leading to faciogenital dysplasia (FGDY; Aarskog-Scott syndrome). FGDY is an X-linked developmental disorder that is characterized by a disproportionately short stature and by facial, skeletal, cardiac, ocular and urogenital anomalies (Aarskog, 1970; Scott, 1971). In many cases, it is also accompanied by mental retardation, neuropsychiatric disorders, and behavioral and learning problems (Fryns, 1992). The *FGD1* gene was identified almost 15 years ago, and it encode the 961-amino-acid protein FGD1, which has strong homology to guanine nucleotide exchange factors (GEFs) for Cdc42 (Pasteris *et al.*, 1994).

FGD1 comprises (in order): a proline-rich N-terminal region; adjacent GEF (Dbl-homology, DH) and pleckstrin homology (PH) domains; a FYVE (Fab1p, YOTB, Vac1p, and EEA1)-finger domain; and a second C-terminal PH domain (PH2; Estrada *et al.*, 2001). Most of these structural motifs are known to be involved in signaling and/or subcellular localization. Indeed, most of the FGD1 mutations identified to date are in the DH/PH region (Orrico *et al.*, 2000), the portion of FGD1 that is responsible for the specific activation of the Rho GTPase Cdc42 (the DH domain) and for membrane binding (the PH domain; Estrada *et al.*, 2001).

The mouse orthologue of the FGD1 protein, Fgd1 (95% identical), is expressed in regions of active bone formation in the trabeculae and diaphyseal cortices of developing long bones. Postnatally, Fgd1 mRNA has been detected more broadly in skeletal tissue, with a higher signal in the perichondrium, resting chondrocytes and joint capsule fibroblasts. Thus, this pattern of Fgd1 expression correlates with the FGDY skeletal manifestations (Gorski *et al.*, 2000), which themselves define most of the other FGDY-related problems.

This article was published online ahead of print in *MBC in Press* (http://www.molbiolcell.org/cgi/doi/10.1091/mbc.E08–11–1136) on March 4, 2009.

Address correspondence to: Roman S. Polishchuk (polish@negrisud.it).

Up-regulation of Fgd1 correlates with an increase in osteopontin, a protein that is specifically expressed in osteoblasts at the onset of matrix mineralization (Gorski *et al.*, 2000).

Given that FGD1 has been localized to the organelles of secretory pathway, including the Golgi complex (Estrada *et al.*, 2001), it might be involved in the regulation of intracellular membrane transport during cell differentiation and therefore be required for normal morphogenesis of bone tissue. Importantly, the main FGD1 target, Cdc42, has a fundamental role in the coordination of membrane transport events, via reorganization of the cytoskeleton and other signaling events (Erickson and Cerione, 2001). In this way, Cdc42 coordinates various aspects of membrane transport, including kinetics (Musch *et al.*, 2001) and fidelity (Kroschewski *et al.*, 1999; Musch *et al.*, 2001) of post-Golgi transport and protein targeting to different surface domains in polarized cells (Kroschewski *et al.*, 1999; Musch *et al.*, 2001).

Interestingly, both FGD1 (Estrada *et al.*, 2001) and Cdc42 (Erickson *et al.*, 1996) have been shown to be associated with the membranes of the Golgi complex, the organelle that has a central role in the control of intracellular membrane transport fluxes. Thus, as an activator of Cdc42, FGD1 should be extremely important in the control of the intensity and vectoriality of membrane trafficking. However, surprisingly, the role of FGD1 in the regulation of membrane trafficking remains completely obscure, with the functional activity of FGD1 only having been examined with regard to the rearrangement of the actin cytoskeleton (Estrada *et al.*, 2001).

Should FGD1 influence the directionality and fidelity of protein transport through its activation of Cdc42, this might be lost in FGDY. Indeed, because polarized secretion of specific proteins is required for correct bone morphogenesis (including collagen-I, osteocalcin, osteopontin, and others; Leblond, 1989) and because the expression of FGD1 strongly correlates with the expression of proteins that are essential for bone development (Gorski *et al.*, 2000), FGD1 appears to have a role in this process Thus, the characterization of FGD1 involvement in the regulation of membrane transport represents an essential task that should have significant importance for our understanding of the pathogenesis of FGDY.

In the present study, after colocalization of FGD1 and Cdc42 to the *trans*-Golgi network (TGN), the "outgoing" compartment of the Golgi complex, we show that inhibition of FGD1 affects post-Golgi transport in general. Furthermore, FGD1 inhibition delays secretion of bone-specific proteins in osteoblasts. These effects on post-Golgi transport depend on FGD1 regulation of the Cdc42 activity and its association with the Golgi membranes and as such might contribute to FGDY pathogenesis.

MATERIALS AND METHODS

Antibodies and Reagents

The following antibodies were used: against TGN46 from S. Ponnambalam (Dundee, United Kingdom); against procollagen-I (PC-I) from L. W. Fisher (Bethesda, MD); against green fluorescent protein (GFP), GM130, giantin, TGN38, osteocalcin, osteonectin, and osteopontin from Abcam (Cambridge, United Kingdom); polyclonal antibody against Cdc42 from Santa Cruz Biotechnology (San Diego, CA); monoclonal antibodies against actin and vesicular stomatitis virus glycoprotein (VSVG) from Sigma-Aldrich (Milan, Italy); polyclonal antibody against FGD1 was produced in our laboratory according to standard protocols. The Alexa 488 and 546 IgG conjugates were from Molecular Probes Europe BV (Leiden, The Netherlands). The Nanogold gold-antibody conjugates and the Goldenhance-electron microscopy (EM) kit were from Nanoprobes (Stony Brook, NY). The cDNA of VSVG-EGFP was from J. Lippincott-Schwarz (National Institutes of Health, Bethesda, MD); cDNA of Cdc42 and its mutants were from A. Hall (Sloan-Kettering Institute, New York, NY); cDNA of TGN38-HRP, designed to anchor the plant enzyme to the targeting sequences from TGN38, was constructed in Colin Hopkins laboratory by Finola Gerachty and was obtained from Dan Cutler (University College London, London, United Kingdom).

RNA Interference, Cell Transfection, and Infection with VSV

HeLa and MC3T3 (clone 4) cells were cultured in DMEM (Invitrogen SRL, San Giuliano Milanese, Italy) supplemented with 10% fetal calf serum and 1 mM L-glutamine. Small interfering RNAs (siRNAs) targeting for either human or mouse FGD1 were obtained from Dharmacon Research (Boulder, CO). siRNAs were transfected as sets of four duplexes (SMARTpool) or as individual duplexes using Oligofectamine (Invitrogen SRL), according to the protocol provided by the manufacturer. Transfection of siCONTROL nontargeting duplexes (Dharmacon) was used as a negative control. Cells were incubated with siRNAs for at least 48 h before further treatments. The efficiency of FGD1 silencing was estimated in each experiment by Western blotting. Lipofectamine 2000 (Invitrogen) was used for cDNA transfections. The infection of cells with VSV was performed as described previously (Polishchuk *et al.*, 2003).

Western Blotting

siRNA-treated HeLa and MC3T3 cells were lysed in 50 mM Tris-HCl, pH 8, containing 0.2% SDS and protease inhibitors. Fifty micrograms of cell lysates were run on 10% SDS-PAGE and transferred to nitrocellulose. Blots were revealed with either anti-FGD1 or anti-actin antibodies using the ECL detection method (Amersham Pharmacia Biotech, Piscataway, NJ).

Cdc42 Activation Assay

The cellular levels of the GTP-bound form of Cdc42 were evaluated with the PAK1-binding assay (Mancini *et al.*, 2003). Briefly, after FGD1-RNA interference (RNAi), HeLa cells were lysed in a Mg^{2+}-based lysis buffer. After centrifugation, the lysates were incubated with the PAK1-p21–binding domain (10 μg GST-PAK1-PBD) and glutathione agarose beads (Amersham Biosciences, Uppsala, Sweden). After 1-h incubation, the PAK1-bound proteins were centrifuged and washed twice in the lysis buffer; then, after boiling in Laemmli sample buffer, they were applied to 12.5% SDS-PAGE and transferred to nitrocellulose. The Western blots were revealed with a rabbit polyclonal antibody against Cdc42, using the ECL detection method.

Immunofluorescence, Confocal Microscopy, and Live-Cell Imaging

For immunofluorescence analyses, the cells were fixed before their incubation with the primary and secondary antibodies of interest. The cells were mounted in mowiol and examined on a Zeiss LSM 510 META confocal microscope (Carl Zeiss, Jena, Germany). All confocal images and time-lapse images were obtained and quantified as described previously (Polishchuk *et al.*, 2003). Overlap between different markers was quantified using the "colocalization" module of the LSM 3.2 software (Zeiss). The tracking of moving objects and evaluation of their speed were performed using the Tracking macro of the ImageJ software (NIH; http://rsb.info.nih.gov/ij/). Selective photobleaching in the regions of interest within the cell was carried out on the Zeiss LSM510 using 100 consecutive scans with a 488-nm laser line at full power. Average fluorescence intensities within regions of interests were quantified using LSM 3.2 software.

Electron Microscopy

Preembedded gold labeling of GFP-FGD1– and Cdc42-GFP–expressing cells was performed according to the nanogold protocol, as described previously (Polishchuk *et al.*, 2003). For visualization of the TGN, HeLa and MC3T3 cells expressing TGN38-HRP were fixed and treated with diaminobenzidine (DAB) using the HRP protocol, as described previously (Polishchuk *et al.*, 2003). The combination of immunogold and HRP methods (nanogold/HRP protocol) was used for double labeling of GFP-FGD1 and TGN38 in TGN38-HRP–expressing cells. In this case after fixing, the cells were incubated first with DAB and then with anti-GFP antibodies, followed by secondary nanogold reagents. Both HRP and gold-labeled cells were embedded in Epon and sectioned on a Ultracut T/FCS microtome (Leica Microsystems S.p.A., Milan, Italy). Immunogold labeling of cryosections with anti-GFP and GM130 antibodies was performed according to previously described procedures (Polishchuk *et al.*, 2003). EM images were acquired from thin sections with a Philips Tecnai-12 electron microscope (Philips, Eindhoven, The Netherlands) using an Ultra View CCD digital camera (Soft Imaging Systems, Munich, Germany). The *trans*-face of the Golgi stack was identified as that containing clathrin-coated membranes and as being at the Golgi pole opposite the *cis*-element of the Golgi stack, which shows a recognizable necklace-like morphology (Rambourg and Clermont, 1990). Quantification of gold particles was carried out using the AnalySIS software (Soft Imaging Systems).

Endo-H Resistance Assay

To determine Endo-H resistance, the cells were initially infected with VSV for 1 h at 32°C. The excess virus was then washed off, and the cells were incubated in DMEM containing 10% HEPES for 2 h at 32°C. The cells were then washed three times with PBS and starved in DMEM without methionine and cysteine for 30 min at 32°C. The cells were then pulsed for 5 min with 200 μCi/ml [^{35}S]methionine in DMEM without methionine and cysteine. To stop the pulse, 10 μl 0.25 M methionine in complete DMEM was added, and the cells were incubated for 2 min at 32°C. A subset of the samples was then transferred to ice, and this was considered time 0. Other samples were washed with complete medium and chased for different times at 32°C. At the end of the chase, the cells were washed once in PBS and lysed in 1 ml lysis buffer (70 mM Tris, pH 7.4, 150 mM NaCl, 0.5% SDS, 1% Triton X-100, 1 mM EDTA, and 1 mM PMSF) and incubated for 60–90 min on ice. The lysates were centrifuged, and the supernatants were incubated with an anti-VSVG antibody overnight at 4°C. The immune complexes were pulled down using protein A-Sepharose. After washing off the unbound material, the protein was eluted by boiling in Endo-H buffer (0.1 M sodium citrate, pH 5.5, 0.5% SDS, and 1% β-mercaptoethanol) for 3–4 min. The eluates were then divided into two tubes, and one was incubated with 40 U Endo-H overnight. The samples were then boiled in SDS-PAGE sample buffer and resolved on an 8% acrylamide gel, using standard procedures. The gels were then scanned and the percentages of the Endo-H–resistant form of VSVG, with respect to the total amounts of VSVG, were quantified using a Fujifilm imager (Tokyo, Japan) or ImageJ software.

PC-I Release Assay

Control and FGD1-silenced MC3T3 osteoblasts were plated as for morphological experiments, washed with fresh medium, and subjected to the 20°C temperature block with the subsequent release for 60 min at 37°C (see *Results*). The incubation media were collected at the end of the 20°C block and then at the end of 60-min incubation at 37°C. Protein in the collected media were precipitated with 10% trichloroacetic acid and analyzed by SDS-PAGE and immunoblotting, using the anti-PC-I antibody at 1:1000 dilution. Immunostained bands of PC-I (160 kDa) were analyzed by ImageJ software. The amounts of PC-I in the samples treated with FGD1-specific siRNAs were normalized to the control.

RESULTS

FGD1 Is Associated with trans-Golgi Membranes

Since the recent demonstration of FGD1 association with Golgi membranes, it has been suggested that it participates in membrane transport events (Estrada *et al.*, 2001). However, to understand which segment of the secretory pathway (endoplasmic reticulum [ER]-to-Golgi, intra-Golgi, or post-Golgi) might be under the control of FGD1, knowledge of its precise localization within the Golgi complex is essential.

To this end, we investigated the distribution pattern of wild-type FGD1 tagged with GFP (GFP-FGD1) in HeLa cells that were labeled with different Golgi markers. Figure 1 shows that GFP-FGD1 is distributed throughout the cell cytoplasm, at the plasma membrane and on the Golgi membranes, as previously reported (Estrada *et al.*, 2001). A more detailed analysis revealed that GFP-FGD1 shows a strong overlap with TGN46 (a TGN marker) in the perinuclear area (Figure 1A, inset). In contrast, GFP-FGD1 colocalization with the *cis*-Golgi protein GM130 was less evident (Figure 1B, inset). Quantification of this GFP-FGD1 colocalization revealed that FGD1 preferentially binds to membranes of the *trans*-Golgi compartment (Figure 1C).

To verify this further, we used an immuno-EM approach. HeLa cells were transfected with GFP-FGD1 and labeled with antibodies against GFP, using the nanogold protocol (Polishchuk *et al.*, 2003). Gold particles indicating GFP-FGD1 were distributed throughout the cell cytosol and were associated with the plasma membrane and intracellular membranes. Comparison of transfected and control cells demonstrated that GFP-FGD1 expression did not induce visible ultrastructural changes in the Golgi complex and other membrane organelles. In the Golgi stacks, FGD1 was mostly on the *trans* cisternae and associated with TGN-like tubular structures (Figure 1D, arrows; see also the quantification in panel G), as confirmed also in cells expressing TGN38-HRP (Figure 1E, arrows) or with double labeling in cryosections (Figure 1F, arrows). In contrast, the *cis* portion of the stack (Figure 1D, arrowheads, and G) was devoid of FGD1 labeling or showed a very weak signal (Figure 1F, arrowheads, and G). Taken together, these observations suggest that FGD1 is involved in membrane transport events at the *trans* side of the Golgi complex.

FGD1 deficit Inhibits Constitutive post-Golgi Transport

To determine whether FGD1 has any role in the export of cargo proteins from the Golgi complex, we used both dominant-positive and dominant-negative forms of FGD1 fused with GFP. For the latter, the GFP-FGD1-AS mutant comprises nearly full-length Fgd1 cDNA that encodes a naturally occurring FGDY-related alternative FGD1 transcript that lacks 36 amino acids in exon 6. This alters the FGD1 DH domain and generates a dominant-negative FGD1 protein that cannot activate Cdc42 (Olson *et al.*, 1996). In contrast, the GFP-FGD1-dbdel fusion construct contains deletions of residues 146-188 and thus removes N-terminal inhibition and results in a constitutively active form of FGD1. This construct also lacks the C-terminal FYVE and PH2 domains, and it is known to constitutively activate Cdc42 (our data, not shown). These FGD1 mutants were used in combination with our well-characterized assay of membrane transport, using the temperature-sensitive ts-O45 mutant of VSV.

HeLa cells expressing GFP-FGD1, GFP-FGD1-AS, or GFP-FGD1-dbdel were infected with VSV and kept at 40°C to accumulate the viral G protein (VSVG) within the ER. The cells were then incubated at 20°C, to trap the VSVG within the Golgi complex. Figure 2, A–C, shows that VSVG was effectively delivered from the ER to the Golgi complex upon expression of each of these FGD1 forms, demonstrating no effects of FGD1 on ER-to-Golgi transport. On the temperature shift to 32°C, in cells expressing wild-type GFP-FGD1 and the active GFP-FGD1-dbdel mutant, VSVG exited the Golgi complex in numerous post-Golgi carriers (PGCs), and was delivered to the plasma membrane (Figure 2, D and F). In contrast, cells expressing GFP-FGD1-AS contained most of the VSVG in the Golgi complex and exhibited much weaker plasma-membrane staining and fewer PGCs (Figure 2E, asterisk).

Tannic acid treatment was then used to block the fusion of PGCs with the plasma membrane (Polishchuk *et al.*, 2004; Jakob *et al.*, 2006), thus resulting in accumulation of these PGCs in the cytoplasm. In nontransfected cells and in cells expressing either the wild-type GFP-FGD1 or the dominant-positive GFP-FGD1-dbdel, numerous PGCs were seen 60 min after VSVG release from the Golgi complex (Figure 2G, I, arrows, and J). However, in cells transfected with the dominant-negative GFP-FGD1-AS, most of the VSVG remained within the Golgi complex, with the number of PGCs strongly reduced (Figure 2H, asterisk, and J), suggesting that the release of VSVG-carrying PGCs from the Golgi complex was inhibited.

Next, to confirm these effects of the dominant-negative FGD1-AS mutant on post-Golgi transport, we silenced FGD1 expression in HeLa cells using RNAi. Treatment of HeLa cells with a pool of four siRNAs directed toward FGD1 (see *Materials and Methods*) induced a significant reduction in FGD1 expression, as revealed by Western blotting (Figure 3A). Moreover, use of a pulldown of Cdc42 by the PAK1-PBD domain (see *Materials and Methods*) revealed that Cdc42 activity in these FGD1-silenced cells was reduced in comparison to cells treated with control siRNAs (Figure 3A).

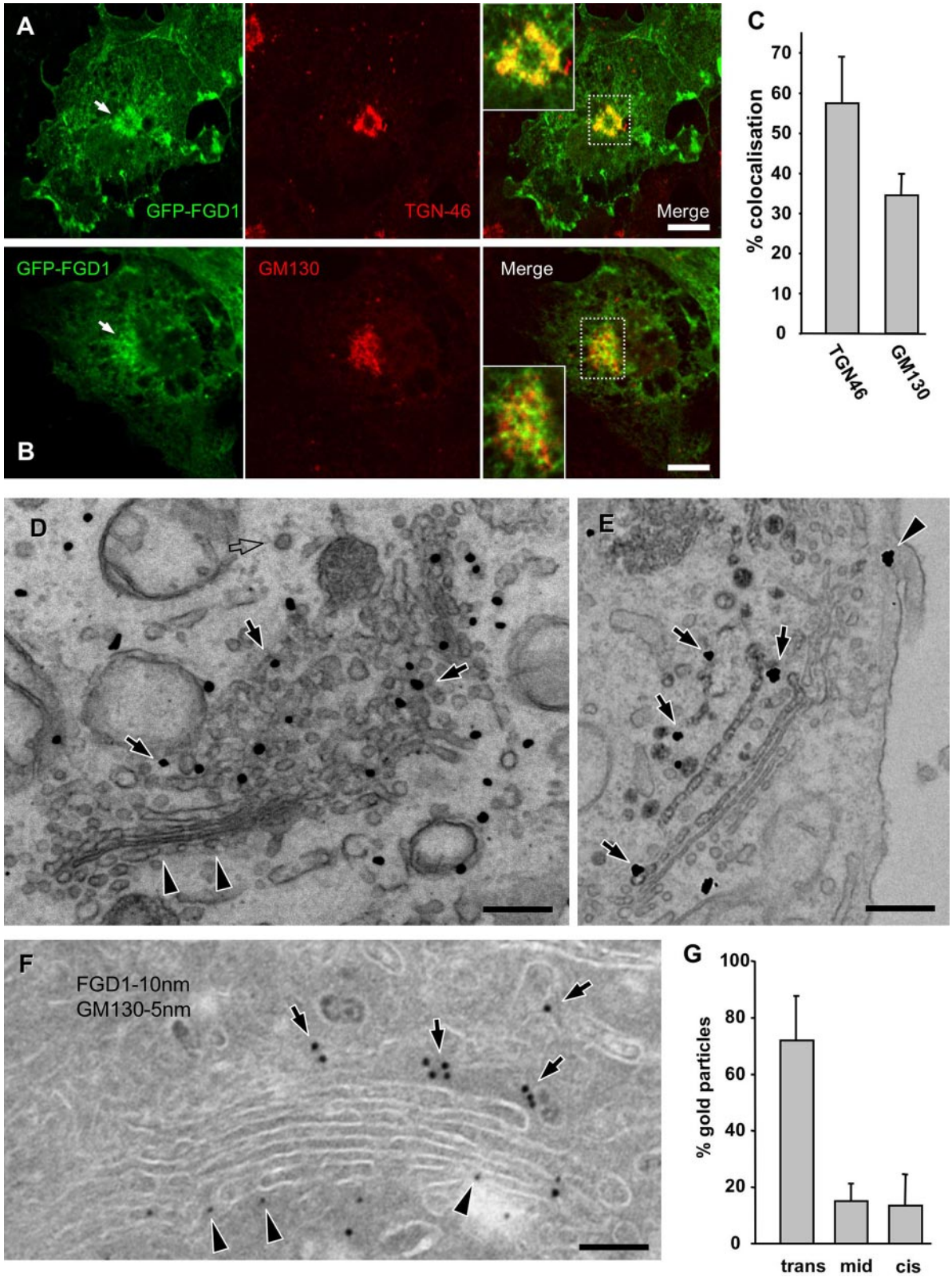

Figure 1. FGD1 at the *trans*-Golgi membranes in HeLa cells. Cells were transfected with GFP-FGD1 (and TGN38-HRP; see panel E), fixed, and either labeled with antibodies against TGN46 (A and C) or GM130 (B and C) and prepared for confocal microscopy (A–C) or labeled with anti-GFP antibodies and prepared for immuno-EM with the nanogold (D), nanogold/HRP (E), or cryo-immunogold (F) protocols (see *Materials and Methods*). (A and B) GFP-FGD1 shows better overlap with the *trans*-Golgi marker TGN46 (A, merge inset) than with the *cis*-Golgi marker GM130 (B, merge inset). (C) Quantification of GFP-FGD1 colocalization with TGN46 and GM130 as illustrated in A and B (means ± SD; n = 30 cells) reveals better overlap with TGN46. (D) Filled arrows indicate FGD1 labeling along tubular-reticular membranes of the TGN; arrowheads indicate necklace-like *cis*-element of the Golgi stack; empty arrow indicates clathrin-coated profile as a typical feature of the

Thus this RNAi of FGD1 also provided us with an effective tool to inhibit FGD1 activity.

To investigate the effects on membrane transport produced by this absence of FGD1, control and siRNAs-silenced HeLa cells were infected with VSVG and subjected to the 20°C block. Figure 3 shows that at the end of the temperature block, in both the control and the silenced cells, VSVG overlapped strongly with the *trans*-Golgi marker TGN46 (Figure 3, B and E). This suggests that this lack of FGD1 does not affect cargo flow to and through the Golgi complex. Indeed VSVG glycosylation in the Golgi complex (evaluated as its processing to the Endo-H–resistant form) was not affected in FGD1-deficient cells (not shown). On warming the cells up 32°C, in control cells, VSVG was effectively delivered to the plasma membrane (Figure 3C), whereas the siRNAs treatment significantly reduced VSVG export from the Golgi complex to the plasma membrane (Figure 3F). Indeed, even 60 min after the release of the 20°C block, the silenced cells had most of their VSVG within the Golgi complex, with very poor plasma-membrane labeling seen (Figure 3F). Other segments of the secretory pathway, such as ER-to-Golgi and intra-Golgi transport, were not to affected by this FGD1 siRNAs treatment, as also seen for the endocytic uptake of epidermal growth factor and WGA lectin (not shown).

To measure the efficiency of membrane transport after this FGD1 knockdown, control and siRNAs-silenced HeLa cells were also treated with tannic acid during VSVG release from the 20°C block. Under these conditions, the control cells showed numerous VSVG-containing PGCs in the cytoplasm (Figure 3D, arrows), whereas the number of similar structures in the FGD1-silenced cells was significantly lower (Figure 3G, arrows). Quantification of PGC accumulation as a result of tannic acid treatment showed that this lack of FGD1 induced a strong reduction in VSVG carrier formation from the Golgi complex (~70%; Figure 3H). As a consequence, arrival of VSVG at the cell surface was significantly inhibited (Figure 3I). Notably, expression of mouse Fgd1 in silenced cells allowed the rescue of the exit of VSVG from the Golgi complex (Figure 3H). In contrast, expression of the inactive FGD1-AS mutant did not overcome the membrane transport block induced by FGD1 knockdown (Figure 3H).

Thus, taken together, our data suggest that PGC formation from the Golgi complex is inhibited in the absence of active FGD1.

FGD1 Silencing Affects Exit and Translocation of Newly Forming PGCs from the Golgi Complex

The process of PGC morphogenesis comprises three main steps: 1) formation of specialized tubular TGN export domains; 2) extrusion of these domains along microtubules; and 3) fission of the export domains to generate free carriers (Polishchuk *et al.,* 2003). Thus we designed several systems to determine which of these steps was affected by an FGD1 deficit. First, we reasoned that inhibition of the first step of PGC formation should result in a reduction in the tubular membranes in the TGN area, which serve as precursors of transport carriers directed to the plasma membrane. Given that these tubular carrier precursors usually contain bona fide TGN markers (Polishchuk *et al.,* 2003), we used EM to determine whether our FGD1 knockdown affected the morphology of TGN38-positive membranes at the exit pole of the Golgi complex. Thus, control and FGD1-silenced cells were transfected with a TGN38-HRP construct and processed for EM, with HRP detection according to the DAB protocol (Polishchuk *et al.,* 2003). Investigation of thin sections revealed TGN38-HRP within the last cisternae of the stack and in several flanking tubular and round profiles (Figure 3J, arrows). Silenced cells, however, had a much larger TGN, which in addition to the cisternae, comprised numerous and extensive tubular profiles (Figure 3K, arrows). Thus, formation of tubular membranes in the TGN area does not appear to be affected by FGD1 depletion. In contrast, these ultrastructural features suggest that it is the consumption of these tubular TGN membranes as transport carriers that is inhibited.

Thus, we used live-cell imaging of cells transfected with VSVG-GFP to determine whether the extrusion of PGC precursors and their fission from the Golgi membranes require FGD1. In control cells, the formation of PGCs often occurs from long (2–10 μm) tubular protrusions that bud from the Golgi complex (Figure 4, A and C, arrows; corresponding Movie 1), which is consistent with previous observations (Kreitzer *et al.,* 2000; Polishchuk *et al.,* 2003). In contrast, FGD1-deficient cells showed only short protrusions coming out from the Golgi complex, and these frequently retracted back into the Golgi without detachment of free transport carriers (Figure 4, B and D; arrows; corresponding Movie 2). Correspondingly, the rate of PGC formation was lower in these FGD1-silenced cells (Figure 4I).

We then analyzed the patterns of PGC movement. Figure 4E shows a projection of the time frames taken each second within the same cell, over a period of ~5 min. As can be seen, moving PGCs produce easily recognizable tracks (Figure 4E, arrows) that can be automatically traced by ImageJ software (Figure 4E, colored lines). Thus, in control cells, when the transport carriers move from the Golgi complex, they do so mostly in a centrifugal direction, along quite straight trajectories (Figure 4E, arrows and colored lines; see also Movie 3). However, only a few of the PGCs seen in FGD1-deficient cells showed a similar behavior (Figure 4F, blue line), with most of the PGCs frequently changing direction or hovering around the Golgi area (Figure 4F, red and green lines; Movie 4). Therefore, it was almost impossible to see trajectories of individual PGCs in projection here (see area indicated by arrowheads in Figure 4F). As a result, the overall distance of PGC movements (Figure 4G) and their speed (Figure 4H) were significantly reduced by this FGD1 knockdown. Thus, FGD1 appears to be required for the pulling of PGCs from the Golgi complex and for their further movement along microtubules toward the cell surface.

FGD1 Is Required for Transport of Bone Proteins in Osteoblasts

Next we asked whether FGD1 is required only for transport of cargo such as VSVG or whether it can also regulate export of other cargo proteins that are normally directed toward the cell surface. To address this issue, we wanted to track endogenous cargo proteins different from VSVG in both topol-

Figure 1 (cont). *trans*-Golgi area. (E) Arrows indicate gold particles corresponding to FGD1 at the TGN38-HRP–positive membranes; arrowhead indicates FGD1 labeling at the plasma membrane. (F) Arrows indicate FGD1 labeling (10-nm gold particles) in the *trans* region of the Golgi complex; arrowheads indicate the opposed *cis* side of the stack decorated with GM130 (5-nm gold particles). (G) Quantification of morphometric analysis of GFP-FGD1 signal as illustrated in D. Gold particle locations are expressed as percentages of the total gold particles at the Golgi membranes (means ± SD; n = 20 stacks), and they show the preferential distribution of FGD1 in the *trans*-Golgi region of the stack. Scale bars, (A and B) 7 μm, (D and E) 200 nm, (F) 110 nm.

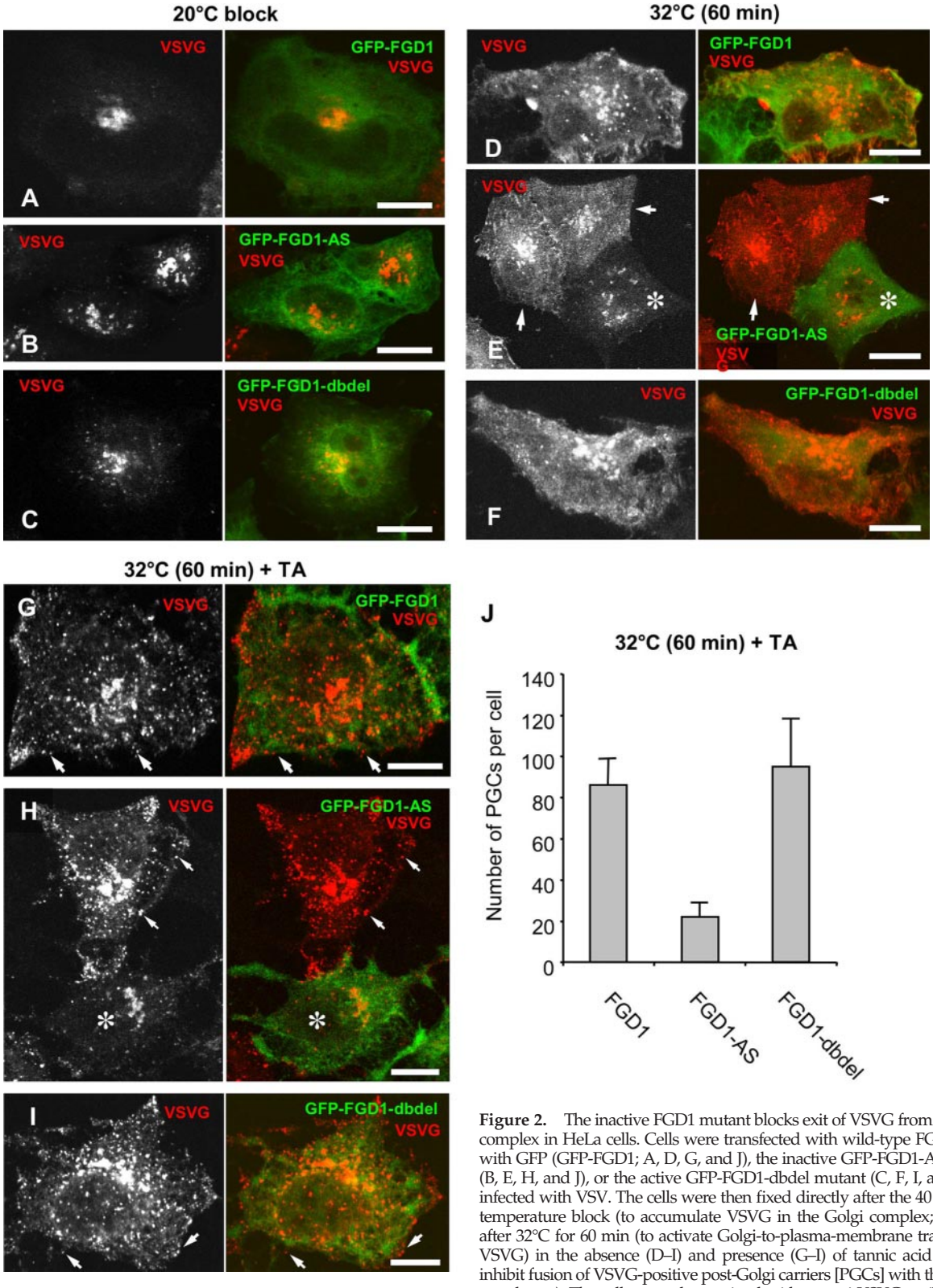

Figure 2. The inactive FGD1 mutant blocks exit of VSVG from the Golgi complex in HeLa cells. Cells were transfected with wild-type FGD1 fused with GFP (GFP-FGD1; A, D, G, and J), the inactive GFP-FGD1-AS mutant (B, E, H, and J), or the active GFP-FGD1-dbdel mutant (C, F, I, and J) and infected with VSV. The cells were then fixed directly after the 40 and 20°C temperature block (to accumulate VSVG in the Golgi complex; A–C), or after 32°C for 60 min (to activate Golgi-to-plasma-membrane transport of VSVG) in the absence (D–I) and presence (G–I) of tannic acid (0.5%; to inhibit fusion of VSVG-positive post-Golgi carriers [PGCs] with the plasma membrane). The cells were then stained with an anti-VSVG antibody and examined under confocal microscopy. (A–C) Expression of all FGD1 isoforms allows accumulation of VSVG within the Golgi complex with the 20°C block. (D–F) On release of the 20°C block VSVG appeared at the plasma membrane of nontransfected cells (e.g., E, arrows) and of cells expressing GFP-FGD1 (D) or GFP-FGD1-dbdel (F). In GFP-FGD1-AS–transfected cells, VSVG remained mainly within the Golgi complex (E, asterisks). (G–I) On release of the 20°C block in the presence of tannic acid, numerous PGCs (G–I, arrows) were seen in nontransfected cells (e.g., H, arrowheads), and in cells expressing GFP-FGD1 (G) or GFP-FGD1-dbdel (I). In GFP-FGD1-AS–transfected cells (H, asterisk), most of the VSVG remained within the Golgi complex. (J) Quantification of PGCs per cell (mean ± SD; n = 30 cells), as illustrated in G–I. A reduction in VSVG carrier formation is seen upon expression of the inactive GFP-FGD1-AS mutant. Scale bars, (A, C, D, and F) 22 μm, (B and E) 30 μm, (G–I) 20 μm.

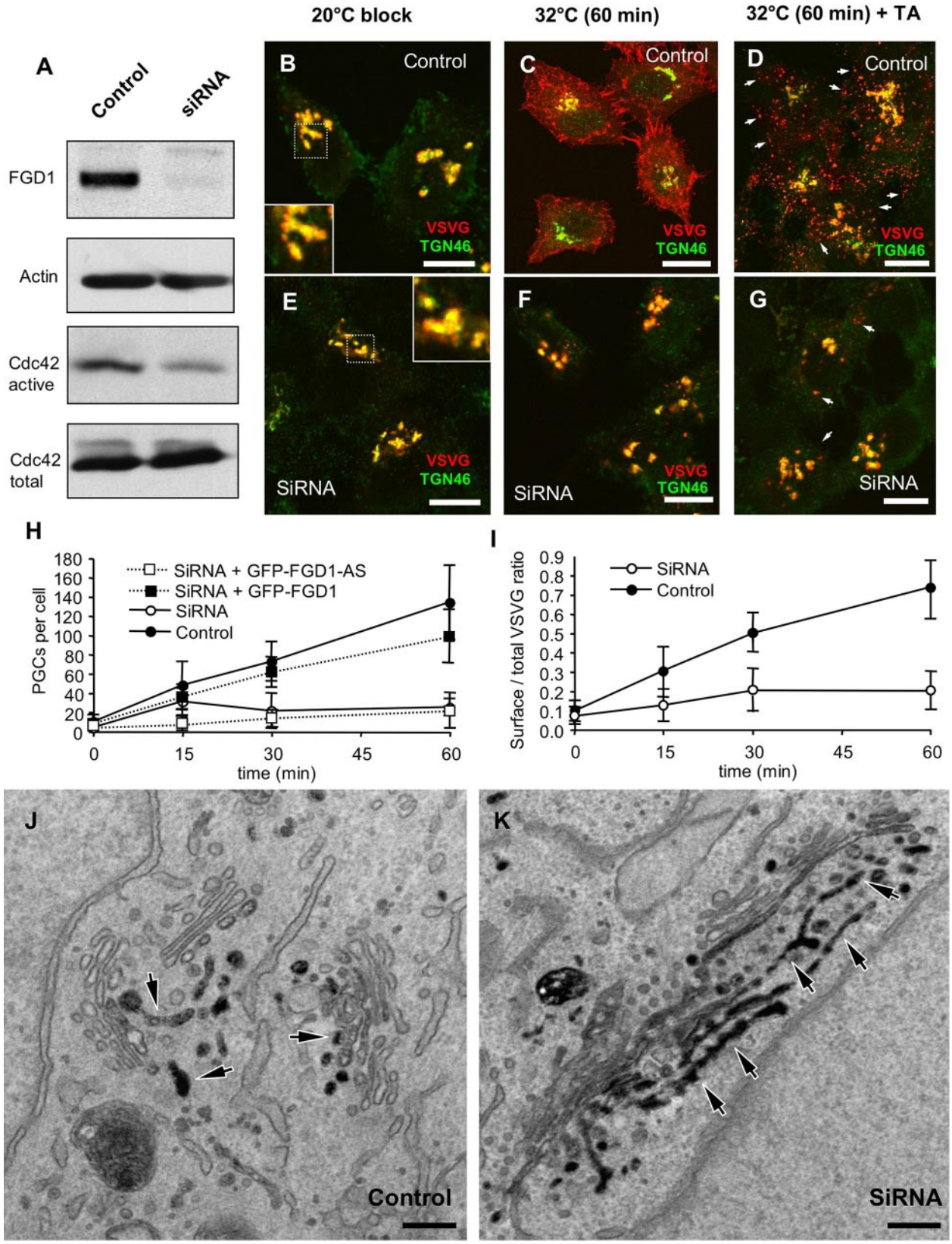

Figure 3. FGD1 silencing inhibits transport from the Golgi complex to the cell surface in HeLa cells. Cells were incubated with an siCONTROL nontargeting duplex (A–D and H–J) or FGD1-specific siRNAs (A, E–I, and K) for 72 h. The cells were then fixed directly to reveal FGD1 expression (A) or infected with VSV and subjected to the 40 and 20°C temperature blocks (B–I), or transfected with cDNA encoding TGN38-HRP (J and K) and processed for electron microscopy according to the HRP protocol (to reveal the TGN; see *Materials and Methods*). (A) Western blotting shows a reduction in FGD1 expression in cells incubated with FGD1-specific siRNAs and a decrease in the active Cdc42

ogy and size. Considering that FGD1 is strongly expressed in bone tissue (which, therefore, is the main target in FGDY pathogenesis), we investigated the transport of major bone proteins, including PC-I, osteocalcin, osteopontin, and osteonectin, in osteoblasts. All of these proteins are soluble (i.e., reside in the lumen of secretory compartments), and therefore they have a topology different from that of VSVG (which is a transmembrane protein). Moreover, they are of different sizes, being either relatively small (osteocalcin, osteonectin, and ostopontin; Lian *et al.,* 1978; Termine *et al.,* 1981; Oldberg *et al.,* 1986) or forming large supramolecular aggregates within early compartments of the secretory pathway (PC-I; Leblond, 1989). All of these proteins have fundamental roles in bone morphogenesis. Thus, we investigated whether membrane trafficking of these proteins is affected by FGDY-related mutations in osteoblasts.

To this end, we studied the transport of PC-I in MC3T3 mouse osteoblasts expressing these FGD1 mutants. MC3T3 cells transfected with the different FGD1 constructs (see above) were subjected to the 20°C block (Polishchuk *et al.,* 2003) to retain PC-I in the Golgi complex (Supplementary Figure 1, A–C) and then shifted to 37°C. Immunofluorescent labeling showed that in cells expressing either the wild-type or the active FGD1 forms, PC-I was effectively packed into numerous PGCs (Supplementary Figure S1D, F, arrows) and exported toward the cell surface (with little or no PC-I left in the Golgi complex). In contrast, in GFP-FGD1-AS–positive cells, a significant portion of the PC-I was retained within the Golgi complex (Supplementary Figure S1E, asterisks), suggesting that this inactive FGD1 mutant inhibits PC-I exit from the Golgi complex. Morphometric analysis confirmed that cells expressing FGD1-AS produced less PC-I–positive carriers in comparison with control cells (Supplementary Figure S1G). Therefore, the expression of the FGD1 mutant, which cannot activate Cdc42, impaired post-Golgi transport of PC-I.

To determine whether transport of other bone proteins is sensitive to FGD1 deficit, we transfected osteoblasts with the different FGD1 constructs and investigated the patterns of osteocalcin, osteonectin, and osteopontin distribution by confocal microscopy. In MC3T3 cells grown under steady-state conditions (i.e., at 37°C, without temperature blocks), osteocalcin was detected within the Golgi complex and in numerous PGCs (Supplementary Figure S1, H and J); this pattern of osteocalcin staining was not affected by expression of either GFP-FGD1 (Supplementary Figure S1H) or GFP-FGD1-dbdel (Supplementary Figure S1J). In contrast, GFP-FGD1-AS–positive cells showed osteocalcin mostly located in the Golgi complex, whereas there was a significant reduction in the number of, and almost a total loss of, PGCs (Supplementary Figure S1I). Similar results were obtained with both osteonectin and osteopontin (not shown). Thus, a loss of FGD1 activity inhibits the export of specific bone proteins in osteoblasts.

To support this conclusion using an independent approach, we used the siRNAs specific for mouse FGD1. Both the control cells and FGD1-silenced cells were subjected to the 20°C block (Figure 5, A and B). In control cells, after the block release, numerous PGCs carrying PC-I were seen throughout the cytoplasm (Figure 5C, arrows). In contrast, in the silenced cells, the FGD1 deficit resulted in a strong inhibition of PC-I exit from the Golgi complex and therefore in a reduction of the number of PGCs (Figure 5, D and E). As a result, PC-I release from FGD1-depleted osteoblasts into the medium was significantly reduced (Figure 5, F and G; see also silencing efficiency in Figure 5H). The inhibitory effects of FGD1 knockdown on PC-I exit from the Golgi complex was also easily detectable at the EM level. Within the Golgi complex, PC-I forms large aggregates, and therefore it resides within large (300–400 nm long; ~150 nm wide) membrane distensions that can be easily detected in thin sections (Leblond, 1989). Control MC3T3 osteoblasts generally showed just a few distensions in the TGN area (Figure 5I, arrows; labeled with the TGN38-HRP construct). In contrast, numerous PC-I distensions were accumulated along the *trans* face of the Golgi stacks upon FGD1 knockdown (Figure 5J, arrows). In addition, the other cisterna of the Golgi complex had more distensions, indicating that FGD1 deficit does indeed induce a PC-I "traffic jam" at the level of exit from the Golgi complex.

Thus, our findings here demonstrate that FGD1 is required for efficient secretion of extracellular matrix proteins by cells of bone origin. Therefore, the absence of a fully functional FGD1 protein might result in the aberrant development of bone tissue, which would be consistent with the FGDY phenotype.

Expression of GDP-bound Cdc42 Mimics FGD1 Deficit

Given that FGD1 has specific GEF activity toward Cdc42 (Olson *et al.,* 1996), we reasoned that Cdc42 activation might be inhibited in FGDY, where the GEF activity of FGD1 is missing. Activation of Cdc42, in turn, is known to be required for the delivery of many proteins to the cell surface (Kroschewski *et al.,* 1999; Musch *et al.,* 2001). Therefore, the lack of active Cdc42 might inhibit membrane transport in a way similar to that of the FGD1 deficit. We thus explored this possibility in detail, using overexpression of a GDP-locked Cdc42T17N mutant as the "classical" tool for the selective inhibition of endogenous Cdc42 activity (Feig, 1999).

Figure 3 (cont). fraction (pulled down using the PAK1-PBD domain; see *Materials and Methods*). Actin expression and total Cdc42 were not affected. (B–I) After the 40 and 20°C temperature block, the cells were fixed directly (to accumulate VSVG in the Golgi complex; B, E, H, and I), or after 32°C for 60 min (to activate Golgi-to-plasma-membrane transport of VSVG) in the absence (C, F, and I) and presence (D, G, and H) of tannic acid (0.5%; to inhibit fusion of VSVG-positive post-Golgi carriers [PGCs] with the plasma membrane). (B–G) The cells were double-labeled for VSVG and TGN46 and examined under confocal microscopy. VSVG accumulation within the Golgi complex during the 20°C block was detected both in control (B) and FGD1-silenced cells (E). Moreover, overlap with TGN46 (insets in B and E) suggests that VSVG moved efficiently across the Golgi complex even with FGD1 silencing. Sixty minutes after release of the 20°C block, VSVG appeared at the plasma membrane of control cells (C), but remained within the Golgi complex in FGD1-silenced cells (F). With tannic acid during this VSVG release, there were numerous PGCs in control cells (D, arrows), whereas FGD1-silenced cells showed only a few (G, arrows). (H) Quantification of time course of PGCs per cell (means ± SD; n = 30 cells) after 20°C block release shows a reduction in PGCs upon FGD1 knockdown. Budding of VSVG carriers from the Golgi complex in silenced cells was rescued by transfection of GFP-fused wild-type FGD1 (H, ■), but not by expression of the inactive GFP-FGD1-AS mutant (H, □). (I) Quantification of surface VSVG to total VSVG ratio of fluorescence intensities (means ± SD; n = 30 cells) after time course from 20°C block release. The cells were initially stained with an antibody against the ectodomain of VSVG, without permeabilization, to reveal surface VSVG. Then the cells were permeabilized, and labeled again with the anti-VSVG antibody to detect total VSVG, with analysis under confocal microscopy. A strong reduction in VSVG delivery to the plasma membrane is seen in silenced cells. (J and K). FGD1-silenced cells show more extensive TGN profiles (K, arrows) in comparison to control cells (J, arrows). Scale bars, (B and E) 18 μm; (C, D, F, and G) 32 μm; (J and K) 220 nm.

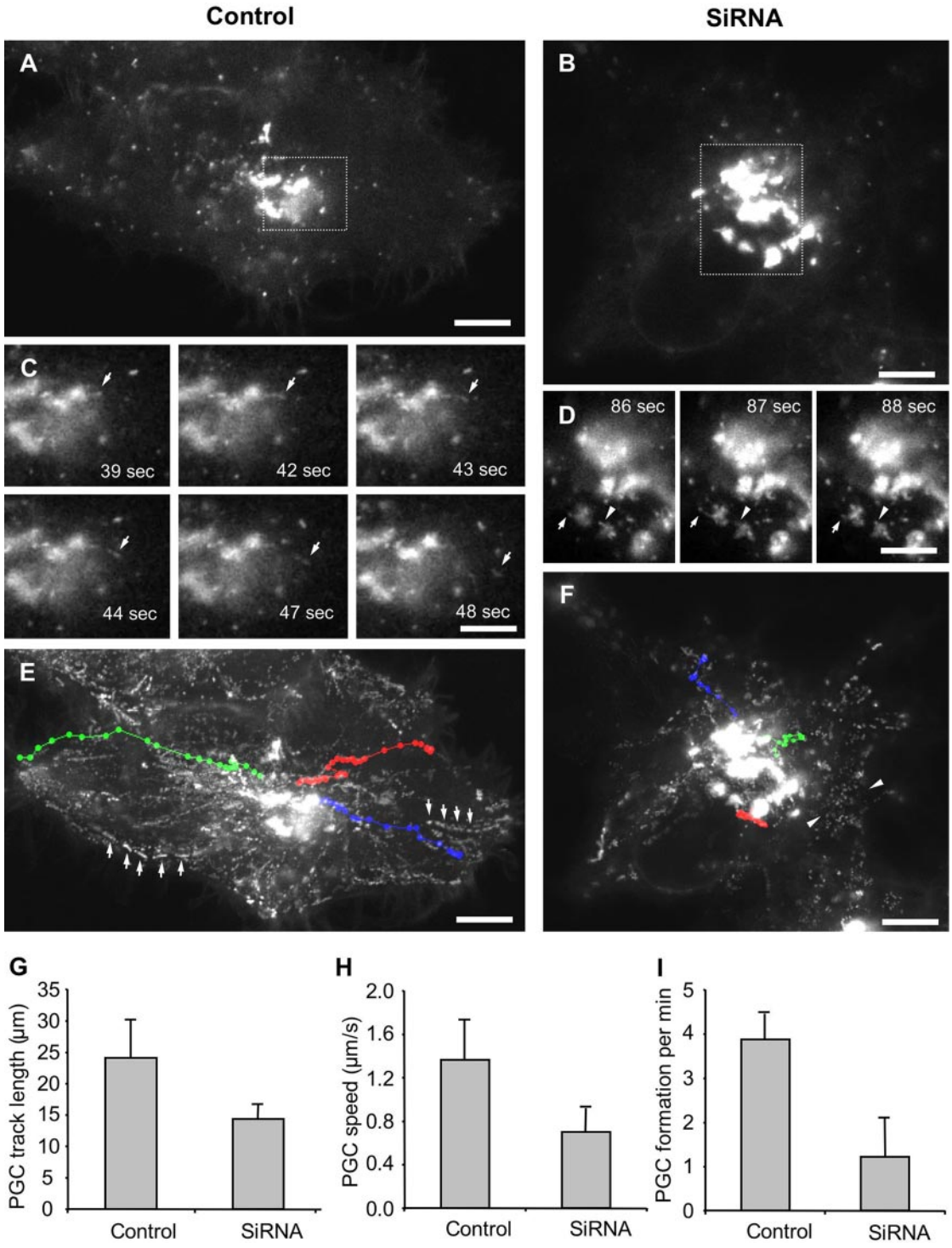

Figure 4. FGD1 silencing blocks exit and translocation of newly forming PGCs from the Golgi complex in HeLa cells. Cells were incubated with an siCONTROL nontargeting duplex (A, C, E, and G–I) or FGD1-specific siRNAs (B, D, F, and G–I) for 72 h. The cells were then transfected with VSVG-GF, subjected to the 40 and 20°C blocks, and examined under confocal microscopy at the permissive temperature of 32°C, with a time resolution of 1 frame per second. (A and B) Exit of PGCs was examined in detail within the Golgi area outlined by dashed boxes in a control (A) and an FGD1-silenced (B) cell. (C and D) Sequential time frames corresponding to the areas indicated in dashed boxes in A and B, respectively. The control cell shows formation of a PGC from a long tubular precursor that extended from the Golgi complex (C, arrow), whereas the FGD1-silenced cell shows extension and retraction of short VSVG-GFP tubules from the Golgi complex (D, arrows and arrowheads). (E and F) Projection of time frames taken each second within the same period of ~5 min in the cells shown in A and B, respectively. (E) In control cells, moving PGCs produce easily recognizable tracks (arrows) that can be automatically drawn by ImageJ software (colored lines). (F) In FGD1-silenced cells, it was almost impossible to detect trajectories of individual PGCs in projection (see area indicated by arrowheads), whereas automatic tracking revealed that most VSVG-GFP carriers frequently changed direction during their movement and hovered around the Golgi area (see red and green lines). (G–I) Morphometric analysis shows that distance of PGC displacement (G), speed of PGC movement (H), and rate of PGC formation from the Golgi (I) were all reduced in FGD1-silenced cells (means ± SD; n = 10 cells). Scale bars, (A, B, E, and F) 16 μm, (C, D) 8 μm.

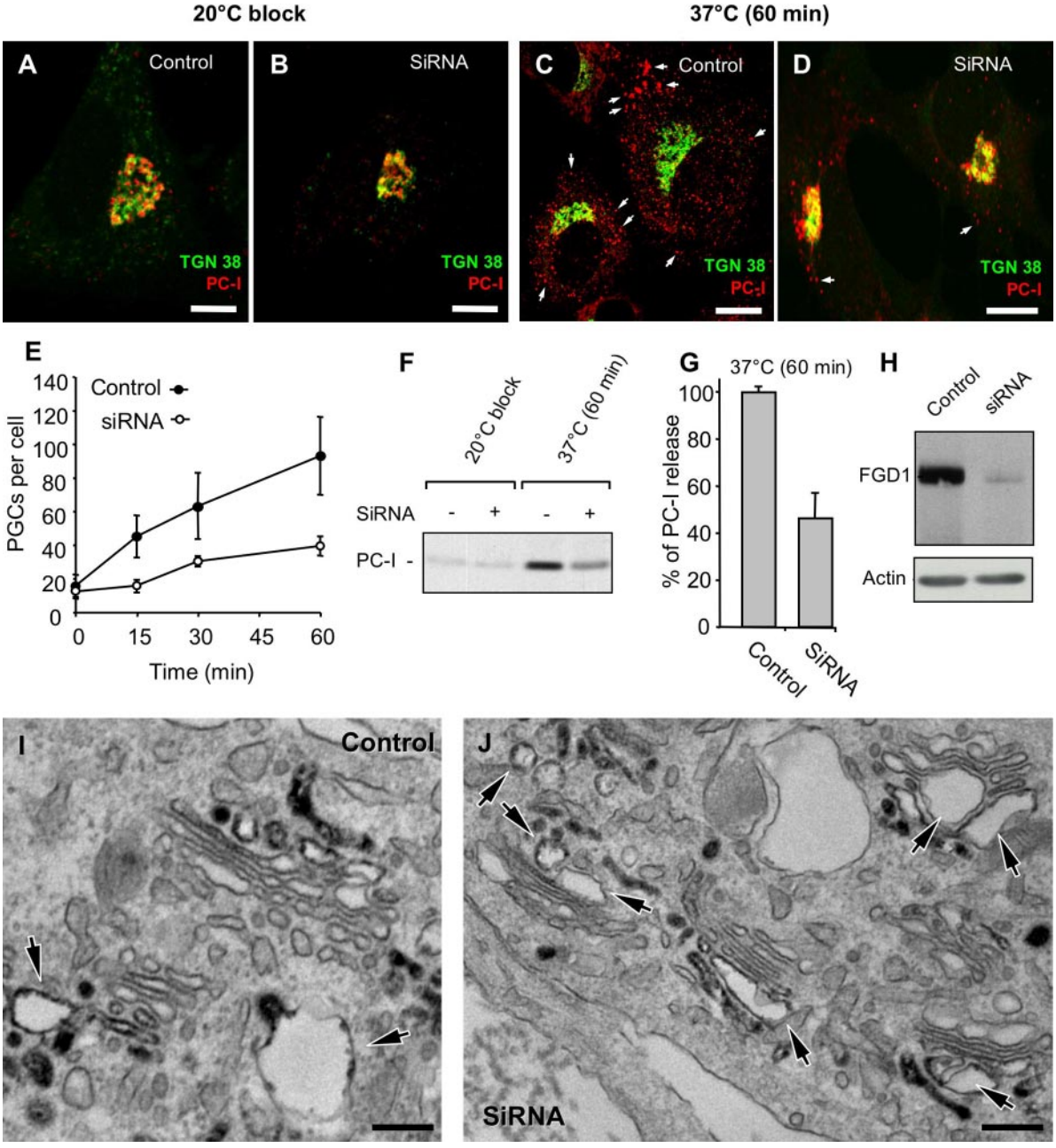

Figure 5. FGD1 silencing induces retention of bone-specific proteins in the Golgi complex of MC3T3 osteoblasts. Cells were incubated with an siCONTROL nontargeting duplex (A, C, and E–I) or FGD1-specific siRNAs (B, D, E–H, and J) for 72 h. The cells were then exposed to the 40 and 20°C blocks (with 50 μg/ml ascorbic acid at 20°C) and then fixed directly (A, B, E, and F) or shifted to 37°C for up to 60 min (C–G; as indicated) or transfected with cDNA encoding TGN38-HRP (I and J) and processed for EM according to the HRP protocol (to reveal the TGN; see *Materials and Methods*). (A–D) The cells were then double-labeled with anti-PC-I and anti-TGN38 antibodies and examined under confocal microscopy. PC-I accumulated within the Golgi complex during the 20°C block in both control (A) and FGD1-silenced cells (B). On release of the block, in control cells PC-I appeared within numerous PGCs (C, arrows), whereas in FGD1-silenced cells only a few PGCs were seen (D, arrows), with most of the PC-I blocked within the Golgi complex. (E) Quantification of time course of PGCs per cell after the 20 C block release (means ± SD; n = 30 cells) shows a reduction in PC-I carrier formation upon FGD1 knockdown. (F) Concomitant release of PC-I into the medium by control and FGD1-silenced osteoblasts was evaluated using a biochemical approach (see *Materials and Methods*). Western blotting indicates that during the 20°C block equally low amounts of PC-I were detected in the medium from both control and silenced cells, whereas 60 min after temperature shift to 37°C control osteoblasts released a significantly higher quantity of PC-I, in comparison to FGD1-silenced cells. (G) Quantification of PC-I signal from Western blotting (e.g., F) calculated and normalized (as % control) using ImageJ software, showing significant reduction in PC-I release in FGD1-silenced osteoblasts (means ± SD; n = 3 experiments). (H) Western blotting shows a reduction in FGD1 expression in cells incubated with FGD1-specific siRNAs, with no effects on actin expression. (I and J). Control MC3T3 osteoblasts usually show a few distensions in the TGN (I, arrows), whereas upon FGD1 knockdown multiple PC-I distensions were seen along the *trans* face of the Golgi stack (J, arrows). Scale bars, (A and B) 16 μm; (C and D) 22 μm; (I) 200 nm; (J) 220 nm.

First, HeLa cells were transfected with myc-tagged wild-type Cdc42 or the myc-tagged Cdc42Q61L (active) and Cdc42T17N (inhibitory) mutants. The cells were then infected with VSVG and subsequently underwent the 20°C temperature block (Supplementary Figure S2, A and B). After the release of the block, VSVG efficiently appeared at the surface of the cells that were positive for Cdc42 (Supplementary Figure S2C) and Cdc42Q61L (not shown). In contrast, expression of the inactive Cdc42T17N inhibited VSVG exit from the Golgi complex and its delivery to the plasma membrane (Supplementary Figure S2D). This observation was also confirmed in tannic acid–treated cells (Supplementary Figure S2, E and F). Furthermore, investigation of PC-I transport in MC3T3 osteoblasts expressing Cdc42T17N also revealed a reduction in PC-I carrier formation from the Golgi complex (Supplementary Figure S2, G and H).

Thus, a block in Cdc42 activity induces an impairment of cargo export from the Golgi complex that is similar to that seen in the absence of the functional Cdc42 activator FGD1. This, in turn, suggests that FGD1 regulates membrane transport through activation of Cdc42.

The localization of Cdc42 would also argue in favor of this hypothesis, as the labeling of Cdc42-transfected cells with different Golgi markers and immuno-EM revealed that Cdc42 associates with TGN membranes (Supplementary Figure S3). This distribution of Cdc42 looked very similar to that of FGD1 and is consistent with the involvement of both of these proteins in the process of cargo exit from the Golgi complex.

FGD1 Regulates Cdc42 Recruitment to Golgi Membranes

Our results here thus indicate that significant fractions of both Cdc42 and FGD1 reside on the Golgi complex and that a loss of either of their activities results in similar inhibitory effects on post-Golgi transport of different cargo proteins. How might FGD1 control Cdc42 activity at the Golgi membranes then? To answer this question, we first asked whether FGD1 and its mutants affect Cdc42 localization at the Golgi complex. Thus, the MC3T3 osteoblasts were cotransfected with Cdc42 and GFP-FGD1 or its mutants: GFP-FGD1-AS and GFP-FGD1-dbdel. The cells expressing GFP-FGD1 showed Cdc42 at the Golgi membranes, at the plasma membrane, and in the cytosol (Figure 6A), whereas the dominant-positive GFP-FGD1-dbdel mutant increased the levels of Cdc42 on Golgi membranes (Figure 6B). In contrast, expression of the dominant-negative GFP-FGD1-AS with its mutation in the Cdc42-activating domain resulted in a redistribution of Cdc42 from the Golgi complex to the cytosol (Figure 6C, asterisks). Of note, the Cdc42 lost from the Golgi complex appeared to be proportional to the GFP-FGD1-AS in the cells, i.e., cells with moderate levels of GFP-FGD1-AS showed residual Cdc42 labeling in the Golgi area, whereas the strong overexpression of this dominant-negative FGD1 mutant saw a complete loss of Cdc42 from Golgi membranes.

Next, Cdc42 association with the Golgi complex was investigated in the FGD1-silenced cells. Thus, MC3T3 osteoblasts were incubated with the FGD1-specific siRNAs and then transfected with either GFP-tagged or myc-tagged Cdc42. Here, the FGD1 knockdown significantly reduced the levels of Cdc42 in the Golgi area (Figure 6, D and E). As for GFP-FGD1-AS expression (see above), these silenced cells showed slightly different phenotypes regarding their Cdc42 pattern. About 60% of the cells completely lost Cdc42 from the Golgi area (Figure 6E, asterisks), whereas some Golgi-localized Cdc42 was still detected in other cells (Figure 6E, arrow). However, in comparison with the control osteoblasts, these FGD1-silenced MC3T3 cells all showed more Cdc42 in the cytosol and less at the Golgi (Figure 6, D and E), with the differences seen in the Cdc42 distributions in these silenced cells explained by different extents of FGD1 knockdown in individual cells.

We then took advantage of the many FGD1-silenced cells that still showed some Cdc42 at the Golgi complex and investigated the kinetics of this Cdc42 association with the Golgi membranes using fluorescence recovery after photobleaching (FRAP). Thus, control and siRNA-treated cells were transfected with Cdc42-GFP, followed by the selective bleaching of the Cdc42-GFP in the Golgi area. The extent of GFP signal recovery was then monitored in these living cells. Figure 6F shows that in control cells the Cdc42-GFP rapidly reappeared at the Golgi (see also Movie 5), whereas in the FGD1-knocked-down cells there was little or no such Cdc42-GFP recovery (Figure 6G; Movie 6). Quantification of these effects revealed that in control cells a significant pool of Cdc42-GFP (~80% of the prebleaching level) was rapidly recovered at the Golgi complex (Figure 6H). In contrast, in silenced cells, only ~30% of the fluorescent signal returned to the bleached Golgi area (Figure 6H).

Thus, the Cdc42 association with the Golgi complex is strongly inhibited when FGD1 is not active.

DISCUSSION

In the present study, we have demonstrated that the Cdc42-specific GEF, FGD1, is involved in the regulation of post-Golgi transport via activation of Cdc42. Both expression of a dominant-negative FGD1 mutant and siRNA-based FGD1 silencing resulted in significant reductions in the delivery of cargo proteins from the Golgi complex to the plasma membrane. This coincided with an impairment of Cdc42 activity and a loss of its association with the Golgi membranes. Moreover, inhibition of Cdc42 itself, by expression of a dominant-negative Cdc42 mutant, resulted in post-Golgi transport aberrations that were similar to those seen under conditions where FGD1 activity was blocked.

These findings have provided us with some insights in our understanding of FGDY pathogenesis, which is known to develop after mutations in the *FGD1* gene in humans (see *Introduction*). Until recently, the issue of how an FGD1 deficit triggers the development of FGDY remained quite elusive. On the basis of its subcellular localization, FGD1 was suggested to participate in both membrane transport and actin remodeling (Estrada *et al.,* 2001), two processes that have fundamental roles in tissue biogenesis. Moreover, use of in situ hybridization has shown that FGD1 mRNA is up-regulated during bone development (and to a lesser extend in other connective tissues), together with a number of proteins that are involved in bone morphogenesis (Gorski *et al.,* 2000). Here, we have shown that FGD1 is required for effective transport of cargo proteins from the Golgi complex to the plasma membrane in general, whereas in osteoblasts it regulates the secretion of PC-I, osteocalcin, osteonectin, and osteopontin. All of these proteins have fundamental roles in the generation of mineralized extracellular matrix during bone development (Lian *et al.,* 1978; Termine *et al.,* 1981; Oldberg *et al.,* 1986; Leblond, 1989), and therefore their aberrant transport through a lack of FGD1 are likely to contribute to the FGDY manifestations.

Because this loss of FGD1 activity that we have achieved through the expression of a dominant-negative FGD1 mutant and through siRNA-based FGD1 silencing, which inhibits post-Golgi transport of various cargo proteins in different cell types, one question that does arise is why an

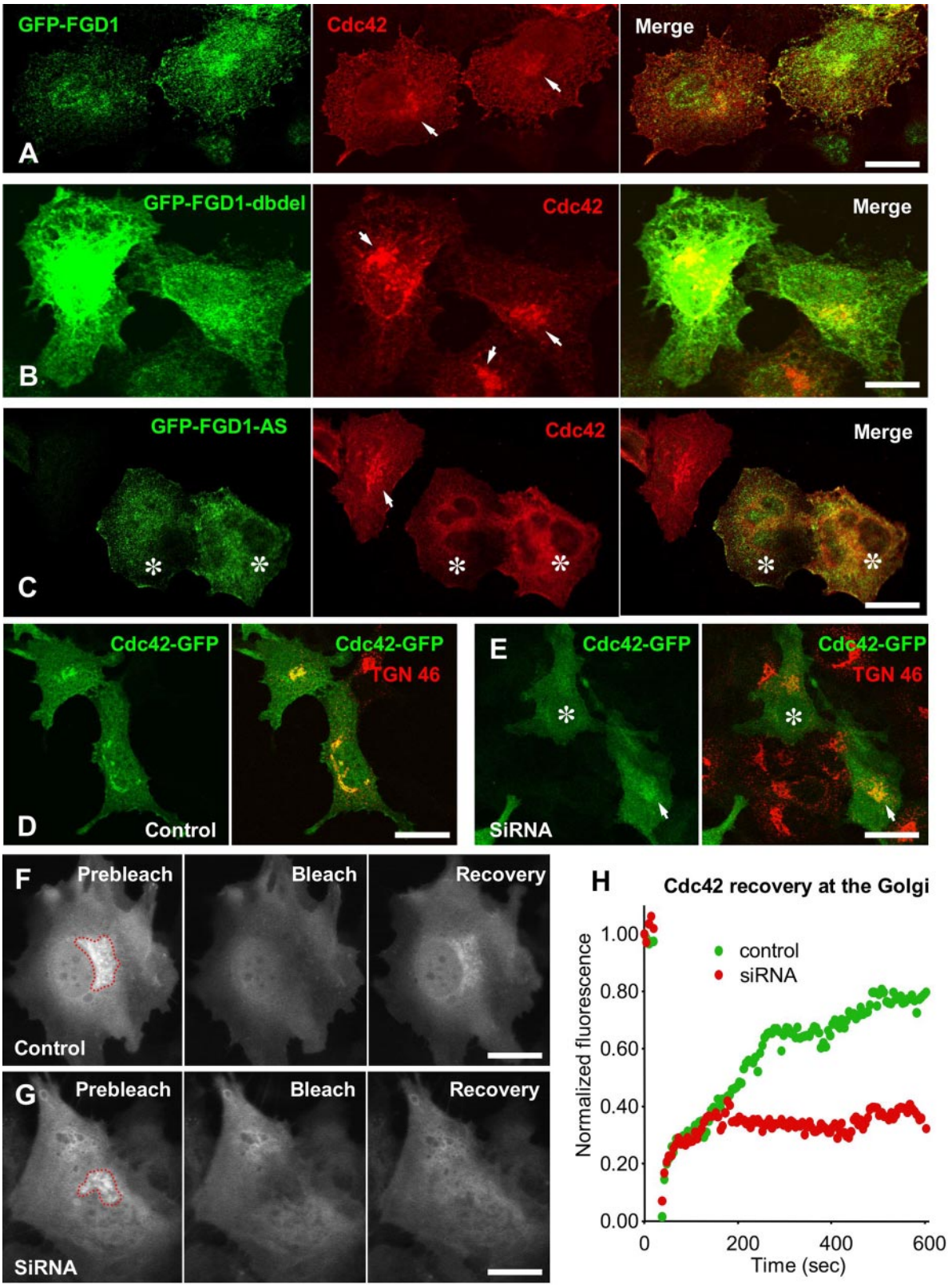

Figure 6. FGD1 regulates Cdc42 recruitment to Golgi membranes in HeLa cells. Cells expressing myc-tagged wild-type Cdc42 (A–C) or Cdc42-GFP (D–H) were transfected with GFP-FGD1 (A), GFP-FGD1-dbdel (B), or GFP-FGD1-AS (C) or incubated with an siCONTROL nontargeting duplex (D, F, and H) or FGD1-specific siRNAs (E, G, and H) for 72 h. (A–C) The cells were fixed and stained with an anti-myc antibody and examined under confocal microscopy. Cdc42 was detected at the Golgi membranes in cells expressing GFP-FGD1 (A, arrows), GFP-FGD1-dbdel (B, arrows) or nontransfected cells (C, arrows), whereas cells transfected with GPF-FGD1-AS (C, asterisks) did not show Cdc42 in the Golgi area. (D and E) The cells were fixed and stained with antibodies against TGN46 and examined under confocal microscopy. In control cells (D), Cdc42 was detectable at the Golgi complex, whereas FGD1-silenced cells either lost Cdc42-GFP from the Golgi membranes

FGD1 mutation affects only some tissues and organs. Apparently this can be explained by a consideration of the expression profile of FGD1: although FGD1 can be detected by Western blotting in cell lines of non-bone origin (e.g., HeLa cells), in situ some tissues (and bone especially) show more FGD1 expression than others (Gorski *et al.,* 2000). FGDY manifestations in the heart and in the urogenital system have also been reported (Scott, 1971) and would correspond to the moderate FGD1 expression seen in these tissues during development (Pasteris *et al.,* 1994).

Several lines of evidence now indicate that FGD1 can regulate post-Golgi transport via activation and recruitment of Cdc42 to the Golgi complex. This began with the localization of both FGD1 and Cdc42 at the Golgi membranes (Erickson *et al.,* 1996; Estrada *et al.,* 2001), and we have shown here that a loss of the activities of either FGD1 or Cdc42 results in similar aberrant transport phenotypes. Furthermore, FGD1 inhibitors affect both Cdc42 activity (Olson *et al.,* 1996) and Cdc42 binding to the Golgi complex (see Figure 6). Given that Cdc42 can be activated by many different GEFs (Hoffman and Cerione, 2002), why are none of these able to efficiently substitute for FGD1 in the support of post-Golgi transport? The answer appears to be quite simple: FGD1 is unique among the numerous Cdc42 GEFs in that it is clearly detected at the Golgi complex (Estrada *et al.,* 2001; the present study). Moreover, as we have demonstrated, the distributions of FGD1 and Cdc42 over the Golgi membranes have similar patterns, with both proteins enriched at the TGN. Thus the Golgi pool of Cdc42 is likely to be activated by FGD1. In contrast, other GEFs acting on Cdc42 have different subcellular locations; to name but a few: intersectin, betaPIX and Vav are associated with the endocytic system, the plasma membrane, and the nucleus, respectively (see Hoffman and Cerione, 2002 for review). Interestingly, all of these GEFs contain the DH/PH tandem, which in the case of FGD1 appears sufficient to target this protein to the Golgi complex (Estrada *et al.,* 2001). Whether other domains of FGD1 (such as its second PH domain, or its FYVE domain) can strengthen this association of FGD1 with the Golgi complex via interactions with lipids or other proteins remains to be seen. In addition to the DH/PH tandem, other Cdc42 GEFs possess various other modules (e.g., SH3, CH, EH, and C2 domains), that are different from those of FGD1. This would allow diversification of the compartmentalization of each of these Cdc42 activators (Hoffman and Cerione, 2002). Indeed, this specific compartmentalization of GEFs makes sense, as it would allow Cdc42 to be regulated selectively to support specific and local intracellular processes without influencing others. This can also be seen with FGD1 silencing, whereby it does not completely inhibit Cdc42 activation (see Figure 3A), consistent with the concept that other GEFs, which would be more specifically associated with different subcellular compartments, can still support Cdc42 activity.

Apart from its interaction with Cdc42, FGD1 has been shown to interact directly with other proteins, including cortactin and actin binding protein 1 (Abp1), via its proline-rich domain (Hou *et al.,* 2003). Given that cortactin appears to be involved in the regulation of export from the Golgi complex (Cao *et al.,* 2005), this direct FGD1-cortactin interaction potentially has an important role in protein delivery from the Golgi complex to the cell surface. However, this is apparently not the case, as we have also seen here that this FGD1-dbdel mutant that lacks the cortactin/Abp1-binding sites of wild-type FGD1 can still support post-Golgi transport (Figures 2, I and J). This again supports the idea that FGD1 regulates post-Golgi transport via its activation of Cdc42, while the FGD1 interactions with other binding partners appear not to be relevant for protein export from the Golgi complex.

We have shown here that this FGD1/Cdc42 machinery acts specifically in the late segment of the secretory pathway (i.e., in post-Golgi transport). Is this then a unique Golgi-related pathway where FGD1 and Cdc42 cooperate to drive transport events? Our data indicate that secretory proteins reach the distal Golgi compartment even when FGD1 is inhibited, suggesting that FGD1 is not required in either ER-to-Golgi or intra-Golgi steps of the secretory pathway. This is consistent with previous reports that have indicated that activation of Cdc42 is needed mainly to control membrane transport events in the post-Golgi space (Kroschewski *et al.,* 1999; Musch *et al.,* 2001). In addition, Cdc42 has been shown to participate in retrograde transport from the Golgi complex to the ER (Luna *et al.,* 2002). Whether or not FGD1 also acts in this Cdc42-mediated transport step at the ER/Golgi interface remains to be determined.

Mechanistically, how might FGD1/Cdc42 activation regulate export from the Golgi complex? The reduction in the number of PGCs in FGD1-silenced cells indicates that it is their formation from the Golgi complex that is affected. According to a recently proposed "pull-and-cut" model (Polishchuk *et al.,* 2003; Bard and Malhotra, 2006), the process of PGC morphogenesis comprises three main steps: 1) formation of specialized tubular-reticular TGN export domains; 2) their extrusion along microtubules; and 3) their fission to generate free carriers. As revealed by TGN38 staining in FGD1-silenced cells, TGN tubular profiles can easily be seen in the *trans*-Golgi area, indicating that the first step of PGC formation is not affected (see Figure 3K). However, we noted that TGN tubular membranes were more abundant in knockdown cells, possibly as a result of a reduction in TGN consumption through the formation of transport carriers. Indeed, the dynamics of PGC formation were altered by RNAi of FGD1 (see Figure 4). Normally, PGCs form from long tubular protrusions that extend from the Golgi body (Polishchuk *et al.,* 2003). In contrast, the FGD1-silenced cells showed only short protrusions coming out from the Golgi mass, which frequently retracted back into the Golgi area without detachment of free transport carriers. Moreover, even when PGCs did pinch off from the Golgi under RNAi, only a few of these moved in a centrifugal direction toward the cell surface; the others remained to hover around the Golgi area. A similar behavior of PGCs was seen in cells injected with an anti-kinesin antibody (Kreitzer *et al.,* 2000). Therefore, FGD1 appears to be required for the interactions between these tubular TGN membranes and the cytoskeleton elements that are involved in their pulling out of, and later fission from, the Golgi complex.

This TGN tubule–cytoskeleton interaction is thus likely to be mediated by Cdc42 activation, and could involve either actin-related or microtubule-related machineries (Rodri-

Figure 6 (cont). (E, asterisk) or showed a reduced Cdc42-GFP signal in the Golgi area (E, arrow). (F and G) The Cdc42-GFP signal was bleached in the Golgi area (see red dashed line) and its recovery over a period of ~10 min was followed within the bleached region under confocal microscopy (see *Material and Methods*). In the control cells the Cdc42 fluorescence at the Golgi complex rapidly reappeared (F), whereas the FGD1-silenced cells did not show significant recovery of the fluorescent signal (G). (H) Quantification of the normalized fluorescence in the bleached area as illustrated in F and G; means ± SD; n = 10 cells. Strong inhibition of Cdc42-GFP recovery in the Golgi region was seen with FGD1 knockdown. Scale bars, (A and B) 25 μm; (C) 30 μm; (D and E) 42; (F and G) 20 μm.

guez-Boulan *et al.*, 2005). A lack of the correct arrangement of actin filaments in the Golgi area after inhibition of Cdc42 has also been correlated with a decrease in cargo exit from the Golgi complex (Musch *et al.*, 2001). This could affect the dynamic behavior of TGN membranes (Musch *et al.*, 2001) and/or the short-range motility of PGCs (or their precursors) in the Golgi area, with this motility appearing to be mediated by myosin VI and to be required for cargo export toward the cell surface (Buss *et al.*, 1998). Golgi-associated Cdc42 effectors, such as WASP (Luna *et al.*, 2002) and IQGAP (McCallum *et al.*, 1998), are also likely be involved in the regulation of actin dynamics at the Golgi complex, and in addition, PAK1 might control the movement of PGCs via the phosphorylation of myosin VI (Buss *et al.*, 1998).

On the other hand, this FGD1/Cdc42 activity also appears to be required for the docking of forming PGCs onto microtubules (see Figure 4). Extension of the TGN export domains along microtubules represents an important feature of PGC formation, due to the generation of tension along the membrane of the PGC precursors (Polishchuk *et al.*, 2003). Membrane tension, in turn, has been shown to greatly facilitate the fission of membrane carriers from parental membranes (Roux *et al.*, 2006). Importantly, to provide a sufficient number of microtubules for cargo exit, the TGN membranes themselves are capable of nucleating microtubules. This process is carried out by the microtubule-associated protein CLASP, which interacts with the *trans*-Golgi protein GCC185 (Efimov *et al.*, 2007). To regulate microtubule nucleation, CLASP might cooperate with CLIP-170, which itself stabilizes microtubules via binding to IQGAP, and which is under the control of Cdc42 (Fukata *et al.*, 2002). Therefore nascent TGN-derived carriers can easily dock onto microtubule highways for further translocation toward the plasma membrane. It is likely that the inactivation of Cdc42 in FGD1-deficient cells will destabilize the Golgi-associated pool of microtubules, and thus this will prevent PGCs from finding microtubules, and hence from efficiently moving their cargo to the cell surface.

With these hypotheses in mind, further efforts are now needed to complete the identification of the molecular players that are involved in these FGD1/Cdc42-dependent mechanisms that promote the export of cargo proteins from the TGN. The achievement of this objective will provide an advance in our understanding of the mechanisms of membrane transport regulation in general, and of their contribution to the pathogenesis of FGDY.

ACKNOWLEDGMENTS

The authors thank Chris Berrie for critical reading of the manuscript. We acknowledge financial support from Telethon Italy (Grants GGP05044 and GTF05007), AIRC (Milano, Italy), and Italian Health Ministry (Art. 12 bis D.Lvo 502/92). O.A.V. was supported by FEBS Summer Fellowship.

REFERENCES

Aarskog, D. (1970). A familial syndrome of short stature associated with facial dysplasia and genital anomalies. J. Pediatr. *77*, 856–861.

Bard, F., and Malhotra, V. (2006). The formation of TGN-to-plasma-membrane transport carriers. Annu. Rev. Cell Dev. Biol. *22*, 439–455.

Buss, F., Kendrick-Jones, J., Lionne, C., Knight, A. E., Cote, G. P., and Paul Luzio, J. (1998). The localisation of myosin VI at the golgi complex and leading edge of fibroblasts and its phosphorylation and recruitment into membrane ruffles of A431 cells after growth factor stimulation. J. Cell Biol. *143*, 1535–1545.

Cao, H., Weller, S., Orth, J. D., Chen, J., Huang, B., Chen, J. L., Stamnes, M., and McNiven, M. A. (2005). Actin and Arf1-dependent recruitment of a cortactin-dynamin complex to the Golgi regulates post-Golgi transport. Nat. Cell Biol. *7*, 483–492.

Efimov, A. *et al.* (2007). Asymmetric CLASP-dependent nucleation of noncentrosomal microtubules at the trans-Golgi network. Dev. Cell *12*, 917–930.

Erickson, J. W., and Cerione, R. A. (2001). Multiple roles for Cdc42 in cell regulation. Curr. Opin. Cell Biol. *13*, 153–157.

Erickson, J. W., Zhang, C., Kahn, R. A., Evans, T., and Cerione, R. A. (1996). Mammalian Cdc42 is a brefeldin A-sensitive component of the Golgi apparatus. J. Biol. Chem. *271*, 26850–26854.

Estrada, L., Caron, E., and Gorski, J. L. (2001). Fgd1, the Cdc42 guanine nucleotide exchange factor responsible for faciogenital dysplasia, is localised to the subcortical actin cytoskeleton and Golgi membrane. Hum. Mol. Genet *10*, 485–495.

Feig, L. A. (1999). Tools of the trade: use of dominant-inhibitory mutants of Ras-family GTPases. Nat. Cell Biol. *1*, E25–E27.

Fryns, J. P. (1992). Aarskog syndrome: the changing phenotype with age. Am J. Med. Genet *43*, 420–427.

Fukata, M., Watanabe, T., Noritake, J., Nakagawa, M., Yamaga, M., Kuroda, S., Matsuura, Y., Iwamatsu, A., Perez, F., and Kaibuchi, K. (2002). Rac1 and Cdc42 capture microtubules through IQGAP1 and CLIP-170. Cell *109*, 873–885.

Gorski, J. L., Estrada, L., Hu, C., and Liu, Z. (2000). Skeletal-specific expression of Fgd1 during bone formation and skeletal defects in faciogenital dysplasia (FGDY; Aarskog syndrome). Dev. Dyn. *218*, 573–586.

Hoffman, G. R., and Cerione, R. A. (2002). Signaling to the Rho GTPases: networking with the DH domain. FEBS Lett. *513*, 85–91.

Hou, P., Estrada, L., Kinley, A. W., Parsons, J. T., Vojtek, A. B., and Gorski, J. L. (2003). Fgd1, the Cdc42 GEF responsible for faciogenital dysplasia, directly interacts with cortactin and mAbp1 to modulate cell shape. Hum. Mol. Genet *12*, 1981–1993.

Jakob, V., Schreiner, A., Tikkanen, R., and Starzinski-Powitz, A. (2006). Targeting of transmembrane protein shrew-1 to adherens junctions is controlled by cytoplasmic sorting motifs. Mol. Biol. Cell *17*, 3397–3408.

Kreitzer, G., Marmorstein, A., Okamoto, P., Vallee, R., and Rodriguez-Boulan, E. (2000). Kinesin and dynamin are required for post-Golgi transport of a plasma-membrane protein. Nat. Cell Biol. *2*, 125–127.

Kroschewski, R., Hall, A., and Mellman, I. (1999). Cdc42 controls secretory and endocytic transport to the basolateral plasma membrane of MDCK cells. Nat. Cell Biol. *1*, 8–13.

Leblond, C. P. (1989). Synthesis and secretion of collagen by cells of connective tissue, bone, and dentin. Anat. Rec. *224*, 123–138.

Lian, J. B., Hauschka, P. V., and Gallop, P. M. (1978). Properties and biosynthesis of a vitamin K-dependent calcium binding protein in bone. Fed. Proc. *37*, 2615–2620.

Luna, A., Matas, O. B., Martinez-Menarguez, J. A., Mato, E., Duran, J. M., Ballesta, J., Way, M., and Egea, G. (2002). Regulation of protein transport from the Golgi complex to the endoplasmic reticulum by CDC42 and N-WASP. Mol. Biol. Cell *13*, 866–879.

Mancini, R., Piccolo, E., Mariggio, S., Filippi, B. M., Iurisci, C., Pertile, P., Berrie, C. P., and Corda, D. (2003). Reorganization of actin cytoskeleton by the phosphoinositide metabolite glycerophosphoinositol 4-phosphate. Mol. Biol. Cell *14*, 503–515.

McCallum, S. J., Erickson, J. W., and Cerione, R. A. (1998). Characterisation of the association of the actin-binding protein, IQGAP, and activated Cdc42 with Golgi membranes. J. Biol. Chem. *273*, 22537–22544.

Mostov, K., Su, T., and ter Beest, M. (2003). Polarised epithelial membrane traffic: conservation and plasticity. Nat. Cell Biol. *5*, 287–293.

Musch, A., Cohen, D., Kreitzer, G., and Rodriguez-Boulan, E. (2001). cdc42 regulates the exit of apical and basolateral proteins from the trans-Golgi network. EMBO J. *20*, 2171–2179.

Nelson, W. J. (2003). Adaptation of core mechanisms to generate cell polarity. Nature *422*, 766–774.

Oldberg, A., Franzen, A., and Heinegard, D. (1986). Cloning and sequence analysis of rat bone sialoprotein (osteopontin) cDNA reveals an Arg-Gly-Asp cell-binding sequence. Proc. Natl. Acad. Sci. USA *83*, 8819–8823.

Olson, M. F., Pasteris, N. G., Gorski, J. L., and Hall, A. (1996). Faciogenital dysplasia protein (FGD1) and Vav, two related proteins required for normal embryonic development, are upstream regulators of Rho GTPases. Curr. Biol. *6*, 1628–1633.

Orrico, A., Galli, L., Falciani, M., Bracci, M., Cavaliere, M. L., Rinaldi, M. M., Musacchio, A., and Sorrentino, V. (2000). A mutation in the pleckstrin homology (PH) domain of the FGD1 gene in an Italian family with faciogenital dysplasia (Aarskog-Scott syndrome). FEBS Lett. *478*, 216–220.

Pasteris, N. G., Cadle, A., Logie, L. J., Porteous, M. E., Schwartz, C. E., Stevenson, R. E., Glover, T. W., Wilroy, R. S., and Gorski, J. L. (1994). Isolation and characterisation of the faciogenital dysplasia (Aarskog-Scott syndrome) gene: a putative Rho/Rac guanine nucleotide exchange factor. Cell *79*, 669–678.

Polishchuk, E. V., Di Pentima, A., Luini, A., and Polishchuk, R. S. (2003). Mechanism of constitutive export from the golgi: bulk flow via the formation, protrusion, and en bloc cleavage of large trans-golgi network tubular domains. Mol. Biol. Cell *14*, 4470–4485.

Polishchuk, R., Di Pentima, A., and Lippincott-Schwartz, J. (2004). Delivery of raft-associated, GPI-anchored proteins to the apical surface of polarised MDCK cells by a transcytotic pathway. Nat. Cell Biol. *6*, 297–307.

Rambourg, A., and Clermont, Y. (1990). Three-dimensional electron microscopy: structure of the Golgi apparatus. Eur. J. Cell Biol. *51*, 189–200.

Rodriguez-Boulan, E., Kreitzer, G., and Musch, A. (2005). Organisation of vesicular trafficking in epithelia. Nat. Rev. Mol. Cell. Biol. *6*, 233–247.

Roux, A., Uyhazi, K., Frost, A., and De Camilli, P. (2006). GTP-dependent twisting of dynamin implicates constriction and tension in membrane fission. Nature *441*, 528–531.

Scott, C. I. (1971). Unusual facies, joint hypermobility, genital anomaly and short stature: a new dysmorphic syndrome. Birth Defects Orig. Artic Ser. *7*, 240–246.

Termine, J. D., Kleinman, H. K., Whitson, S. W., Conn, K. M., McGarvey, M. L., and Martin, G. R. (1981). Osteonectin, a bone-specific protein linking mineral to collagen. Cell *26*, 99–105.